Progress In Electromagnetics Research, Vol. 144, 93–101, 2014

Polarization Angle Independent Perfect Metamaterial Absorbers for Solar Cell Applications in the Microwave, Infrared, and Visible Regime

Furkan Dincer[1, 3], Oguzhan Akgol[2, 3], Muharrem Karaaslan[2, 3], Emin Unal[2, 3], and Cumali Sabah[4, *]

Abstract—We design, characterize, and analyze a new kind of metamaterial (MTM) absorber (MA) in different frequency regions for the solar cell applications. This MTM based structure is particularly presented in a range of the solar spectrum in order to utilize the solar energy effectively. The proposed MTM based solar cell provides perfect absorption for both infrared and visible frequency ranges and can be used for the realization of more efficient new solar cells. The structure is also tested in terms of the polarization angle independency. The suggested MA has a simple configuration which introduces flexibility to adjust its MTM properties to be used in solar cells and can easily be re-scaled for other frequency ranges. Our experimental results in microwave frequencies confirm the perfect absorption for the resonance frequency and agree with the simulation results. This means that the developed MA for solar cells will offer perfect absorption in infrared and even in visible frequencies.

1. INTRODUCTION

The solar energy has received considerable attention for the clean energy resource in order to solve the environmental problems and energy needs in the worldwide scale because solar energy is more flexible, environment friendly, cost effective, and commercially widespread. Therefore, the solar energy is widely used today in many applications such as water heating-cooling, cooking, electricity generating, etc. [1, 2]. Solar radiation can be absorbed and converted directly into electrical energy by using solar cells. A solar cell is a device that converts the sunlight energy directly into electricity by the photovoltaic effect. The photovoltaic effect occurs when voltage or current in a material are exposed to solar radiation. When solar energy hits the solar cell, electrons are knocked loose from the atoms in the semiconductor material, creating electron-hole pairs. If electrical conductors are attached to the positive and negative sides of an electrical circuit, the electrons are captured in the form of electric current. The wavelength of the solar radiation mostly ranges from 300 nm to 3000 nm, which means the frequency ranges from 100 THz to 1000 THz [3, 4].

The efficiency of solar cells converting solar radiation to electricity is low and not enough today due to the fact that solar cells are not exactly converting all solar radiation. Solar radiation has wide frequency range, but solar cells can only absorb specific frequency ranges causing inefficiency of solar cells. However, solar cell based MTMs can absorb solar radiation in a wider frequency ranges. Recent studies show that MTMs provide improvement in light collection for solar cells [5–7]. MTMs are artificial structures [8–23] and they can be specifically constructed for many desired physical properties and applications which cannot be obtained from the conventional materials such as negative refractive index [24], cloaking [25], super lens [26], absorber [27], and so on. Therefore, MTMs have gained

Received 14 November 2013, Accepted 23 December 2013, Scheduled 6 January 2014

* Corresponding author: Cumali Sabah (sabah@metu.edu.tr).

[1] Department of Computer Engineering, Mustafa Kemal University, Iskenderun, Hatay 31200, Turkey. [2] Department of Electrical and Electronics Engineering, Mustafa Kemal University, Iskenderun, Hatay 31200, Turkey. [3] Metamaterials and Photonics Research Group, Mustafa Kemal University, Iskenderun, Hatay 31200, Turkey. [4] Department of Electrical and Electronics Engineering, Middle East Technical University, Northern Cyprus Campus, Kalkanli, Guzelyurt, TRNC/Mersin 10, Turkey.

a great deal of interest due to their large applicability in the development of efficient devices. The researchers who study MTMs have also focused on the absorber applications of MTMs as mentioned and there are many MA studies in the literature. These studies are generally constructed in microwave ranges. However, for the last few years, researchers have been studying MTMs for visible and infrared ranges [10–12].

In this study, we design, characterize, and analyze a new kind of MA covering solar spectrum range in order to utilize the solar energy effectively. The new absorber configuration for solar cell applications (based on MTM composed of square resonators with gaps) is designed for microwave, infrared, and visible frequency ranges. In addition, the proposed design is investigated both numerically and experimentally in the microwave region in order to show its performance to be a fundamental structure for other regimes especially for infrared and visible frequency ranges and to be used in solar cells for improving their efficiencies. The proposed novel design has a very simple geometry which allows the simplification in the fabrication process. Proposed structure has also a mechanical tunability feature due to its very flexible design with a single layer. Our designed structure, according to the simulation results, shows a strong resonance and its all versions provide perfect absorption in corresponding microwave, infrared and visible frequency ranges. This is validated by both simulation and experimental studies. To show the applicability of the configuration, experimental results were obtained by manufacturing the designed structure for microwave frequencies (C-band) and it was shown that the experimental results agree with the simulation results obtained by a commercial software leading us to conclude that the designed structure can be used in infrared or even in visible frequencies by simply adjusting its dimensions. The surface current and electric field distributions are also analyzed to demonstrate and verify the physical mechanism of the proposed MTM based absorber.

2. THEORY

As well known, solar cells absorb energy of solar radiation. Since, the generated electricity with solar cells depends on absorption rate of solar radiation, reflection and transmission waves should be minimized ($R(\omega)\,\&\,T(\omega) \rightarrow 0$) as much as possible to achieve a perfect absorption. Reflection-transmission coefficients can be defined from the power flow on the ports as [3];

$$R\left(\omega\right) = \frac{\text{Power reflected from port 1}}{\text{Power incident on port 1}} \tag{1}$$

$$T\left(\omega\right) = \frac{\text{Power delivered to port 2}}{\text{Power incident on port 1}} \tag{2}$$

Absorption level of the solar cells can be calculated by $A(\omega) = 1 - R(\omega) - T(\omega)$, where $A(\omega)$, $R(\omega) = |S_{11}|^2$ and $T(\omega) = |S_{21}|^2$ are the absorption, reflectance, and transmittance at a certain frequency range, correspondingly. There will be no transmission to be examined throughout the present study, as it is blocked off by the continuous metal plate. Therefore, only the reflection needs to be investigated which is directly related with S_{11}. Consequently, the absorption can be calculated as $A(\omega) = 1 - R(\omega)$. The absorption may achieve unity when the reflection is very close to zero which is the main aim of the study. This purpose can be accomplished by using MTM structure(s) in solar cells as mentioned before. Simply, MTMs can be characterized by a complex frequency dependent electric permittivity $\tilde{\varepsilon}(\omega) = \varepsilon_1(\omega) + i\varepsilon_2(\omega)$ and a complex frequency dependent magnetic permeability $\tilde{\mu}(\omega) = \mu_1(\omega) + i\mu_2(\omega)$. Reflectivity can also be reduced (near-zero) when the effective permittivity $\tilde{\varepsilon}(\omega)$ and permeability $\tilde{\mu}(\omega)$ have minimum values. Therefore, $\tilde{\varepsilon}(\omega)$ and $\tilde{\mu}(\omega)$ can properly be tuned to absorb both the incident electric and magnetic fields for perfect absorption [16–20].

3. DESIGN, SIMULATION, AND EXPERIMENT

The proposed design consists of a square-shaped resonator with gaps in the unit cell which is shown in Figure 1. The metallic structures on the top and bottom layers of the substrate are chosen as silver sheet with the electrical conductivity of 6.3×10^7 S/m and thickness of 35 nm and 30 nm for infrared and visible ranges, respectively. Silver is a soft, white, lustrous transition metal and possesses extremely low resistivity. The Drude model approximation, in infrared and visible ranges, is used

to describe the effective metallic dielectric properties of the silver metallization which can be given as $\varepsilon(f) = 1 - f_p^2/(jf\gamma + f^2)$, where f_p is the plasma frequency and γ is the damping rate of the material [28–31]. The following values are used for the plasma frequency and damping rate: $f_p = 2180\,\text{THz}$ and $\gamma = 4.35\,\text{THz}$ [28–31]. For microwave frequency range, copper with electrical conductivity of $5.8\times10^7\,\text{S/m}$ and thickness of 0.036 mm are chosen. Copper is commonly used in microwave applications. A square-shaped resonator with gaps on the top and the metal plate on the bottom layer are separated by the Quartz (Fused) dielectric substrate which is selected as a substrate with the thickness of 250 nm and 200 nm for infrared and visible range, respectively. The loss tangent and relative permittivity of the Quartz are 0.0004, and 3.75. A 1.6 mm-FR4 is chosen as dielectric substrate for microwave frequency range. The loss tangent and relative permittivity of FR4 are 0.02 and 4.2, respectively. The dimensions of the simulated unit cells are presented in Figure 1(a) for the infrared, visible, and microwave frequencies, correspondingly. The unit cells have the following periodicities: 2800 nm × 2800 nm for infrared, 1200 nm × 1200 nm for visible, and 30 mm × 30 mm for microwave frequencies. In order to obtain experimental results, the structure is adjusted for microwave frequencies and the fabricated periodic structure is shown in Figure 1(b).

First, the structure is simulated with a commercial full-wave EM solver based on finite integration technique. Periodic and open add space boundary conditions are used in the simulations. The microwave measurement is carried out by using a vector network analyzer (VNA) and two horn antennas with the range of 1 GHz to 6 GHz. The fabricated structure and devices used in the measurement are shown in Figure 2.

4. RESULTS AND DISCUSSION

The numerical and experimental results are related and verified to show the performance of the suggested MA. Simulated and measured reflection and absorption values are presented in Figure 3 and Figure 4

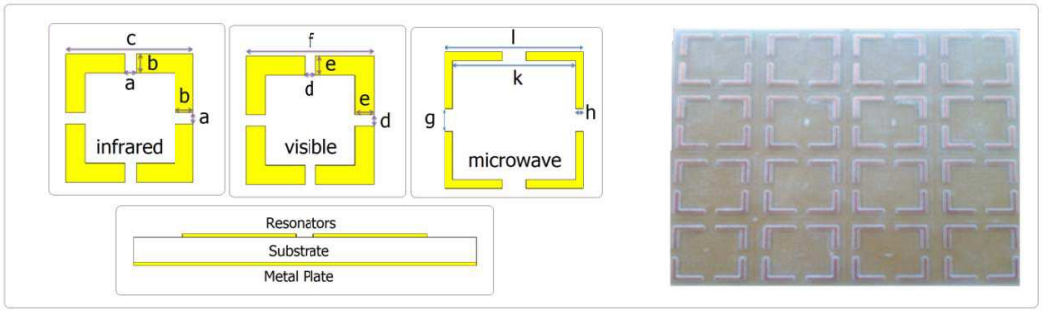

Figure 1. Designed and fabricated absorbers. (a) Unit cells with dimensions for the infrared, visible, and microwave samples; $a = 150$ nm, $b = 300\,\text{nm}$, $c = 2000\,\text{nm}$, $d = 70\,\text{nm}$, $e = 10\,\text{nm}$, $f = 800\,\text{nm}$, $g = 4\,\text{mm}$, $h = 1.5\,\text{mm}$, $k = 21\,\text{mm}$, $l = 24\,\text{mm}$. (b) Fabricated microwave structure with 6 mm cell separation.

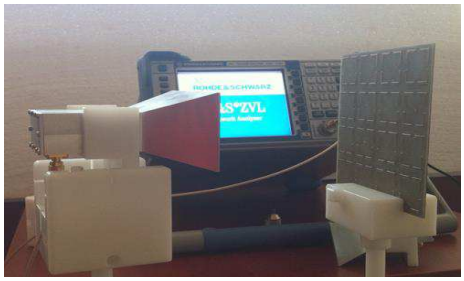

Figure 2. A picture from the experimental study.

for microwave C-band frequency range. Measurement setup is used for verifying numerical results. It can be seen from the simulation that maximum absorption of 99.99% is observed at 4.28 GHz. The corresponding reflection value is 0.002 at that resonance frequency. Maxima in the absorption are experimentally obtained around 99% at 4.35 GHz in which it can be seen that the suggested model shows perfect absorption both numerically and experimentally. Note that, the discrepancies between the experimental and simulation data are imputed to fabrication tolerances and dielectric dispersion of the substrate. The misalignment during the experiment may also be considered as another source of error. The accuracy of the measurements can be clarified by the good agreement between the simulation and experimental results. Therefore, the proposed structure can be used in long-distance radio telecommunications (as directly related with C-band) and it will be a very good candidate for the applications of satellite communication transmissions, some Wi-Fi devices, some cordless telephones, some weather radar systems, etc.

Moreover, we performed some simulations using the suggested structure for infrared and visible frequency ranges. Since the proposed model introduces flexibility to adjust its MTM properties, the structure is easily rescaled for infrared and visible frequency regions. Maximum absorptions for infrared and visible ranges are numerically obtained around 99.66% at 268.82 THz and 99.9% at 542.97 THz as shown in Figure 5 and Figure 6, respectively.

In the next exploration, the effects of the polarization angle on the behavior of the suggested MA are examined for microwave C-band frequency range. The frequency response of the absorption behavior can be seen in Figure 7. It can be clearly seen that the proposed MA structure offers quite well absorption response for various polarization angles in the studied spectrum range. Even though, there are slight shifts depending on the angles, the absorption levels are pretty high and the shift is in the negligible level. This will provide great advantage for solar cell applications since the incident waves will change constantly during the day. With this behavior the structure will remain in the same position and no additional control units would be necessary. Briefly, the solar system would receive maximum level of light absorption during all day when the proposed MA is implemented into the system.

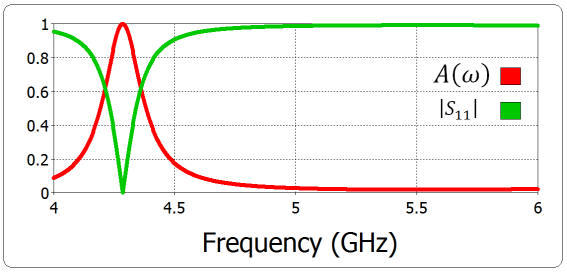

Figure 3. Simulated reflection and absorption of the suggested MA for microwave C-band frequency range.

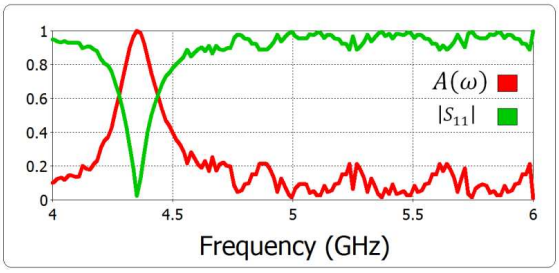

Figure 4. Measured reflection and absorption of the suggested MA for microwave C-band frequency range.

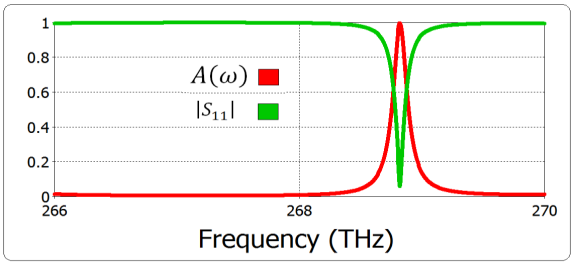

Figure 5. Simulated reflection and absorption at the infrared region to be used in the application of solar cells.

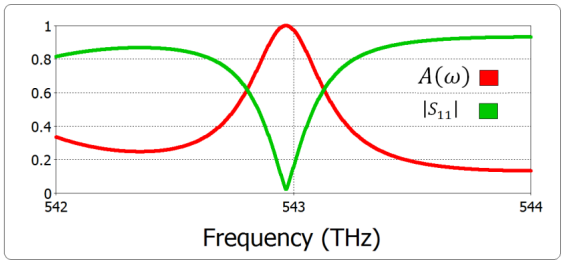

Figure 6. Simulated reflection and absorption at the visible region to be used in the application of solar cells.

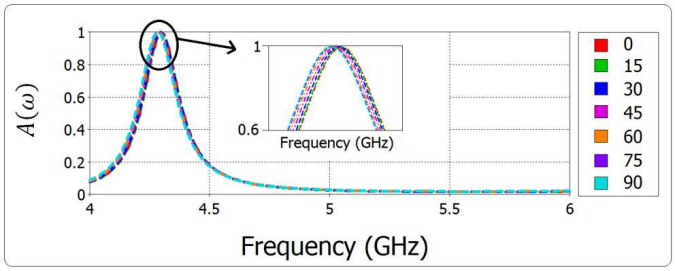

Figure 7. Simulated results of the absorbing performance under different polarization angles in microwave C-band region.

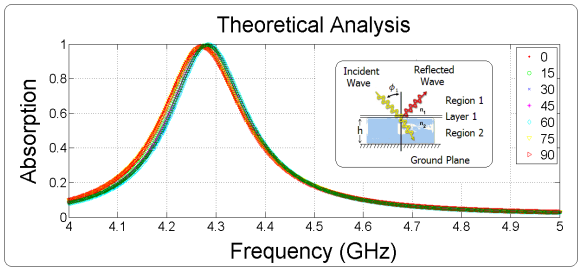

Figure 8. Theoretical results of the absorbing performance under different polarization angles in microwave C-band region.

In order to verify numerical results of the proposed MA for different polarization angles in microwave C-band region, theoretical investigation is performed. The theoretical results are shown in Figure 8. Firstly, we theoretically analyzed the proposed structure for the couple- (conventional metamaterial absorber) and decouple- (metamaterial unit only without ground plane) models in order, at normal incidence. Then, we proposed the extended interference theory model which is applicable to oblique incidence condition. Figure inset of Figure 8 shows the theoretical model. $S_{11} = |s_{11}|e^{j\theta_{11}}$ is the reflection coefficient of layer 1 from region 1 to region 1, $S_{21} = |s_{21}|e^{j\theta_{21}}$ is the transmission coefficient of layer 1 from region 1 to region 2, $S_{12} = |s_{12}|e^{j\theta_{12}}$ is the transmission coefficient of layer 1 from region 2 to region 1, and $S_{22} = |s_{22}|e^{j\theta_{22}}$ is the reflection coefficient of layer 1 from region 2 to region 2. The overall reflection wave of layer 1 from region 1 back to region 1 is can be calculated according to the proposed interference theory for suggested model as [32–35];

$$\sum S_{11} = S_{11} + S_{12}e^{-j(2\beta+\pi)}S_{21} + S_{12}e^{-j(2\beta+\pi)}\left(S_{22}e^{-j(2\beta+\pi)}\right)^1 S_{21} + S_{12}e^{-j(2\beta+\pi)}\left(S_{22}e^{-j(2\beta+\pi)}\right)^2 + \ldots \quad (3)$$

$$\sum S_{11} = S_{11} + S_{12}e^{-j(2\beta+\pi)}S_{21}\sum_{n=0}^{\infty}\left(S_{22}e^{-j(2\beta+\pi)}\right)^n \quad (4)$$

$$\sum S_{11} = S_{11} + \frac{S_{12}e^{-j(2\beta+\pi)}S_{21}}{1 - S_{22}e^{-j(2\beta+\pi)}} \quad (5)$$

$$\sum S_{11} == |s_{11}|\, e^{j\theta_{11}} + \frac{|s_{12}|\,|s_{21}|\, e^{j(\theta_{12}+\theta_{21}-2\beta-\pi)}}{1 - |s_{22}|\, e^{j(\theta_{22}-2\beta-\pi)}} \quad (6)$$

where $\beta = kd$ represents the complex propagation phase, k the wavenumber for region 2, and d the propagation distance of the transmitting wave from layer 1 to ground plane, which can be calculated from Snell's Law (also known as the law of refraction);

$$n_1 \sin\phi_1 = n_2 \sin\phi_2 \quad (7)$$

$$\sin\phi_2 = \frac{n_1 \sin\phi_1}{n_2} = \frac{\sqrt{\varepsilon_1 x \mu_1}\sin\phi_1}{\sqrt{\varepsilon_2\mu_2}} = \sqrt{\frac{\varepsilon_1}{\varepsilon_2}}\sin\phi_1 \quad (\mu_1 = \mu_2) \quad (8)$$

$$\phi_2 = \arcsin\left(\sqrt{\frac{\varepsilon_1}{\varepsilon_2}}\sin\phi_1\right) \quad (9)$$

$$d = h\cos(\phi_2) \quad (10)$$

where ε_1 and ε_2 are permittivities of region 1 and 2, in order; ϕ is the angle between the incidence wave and the normal of the interface; h is the perpendicular distance from layer 1 to ground plane. So, the absorption is then retrieved through $A(\omega) = 1 - |\sum S_{11}|^2$, since the transmission is zero ($T(\omega) = 0$) due to the ground plane. As seen from Figure 8, there is a good agreement between the theoretical and simulation results given in Figure 7. Therefore, the theoretical verification is fulfilled for the proposed configuration.

In addition, it is really important to know the extent up to which this structure can be tuned by simply changing some parameters. Changing the gap (length-g) distance between the branches in the

structure would be enough to shift the resonant frequency to the desired range. Mechanical tunability can also be obtained using a method mentioned in [36]. The effects of changing the gap can be seen in Figure 9. As it can be seen, it is obvious that although the absorption peak moves with the variation of the gap size, the proposed structure maintains a great absorption over a wide range. Note that, the fabrication was realized for the structure providing the best absorption value ($g = 4\,\text{mm}$).

As known, the proposed MA for solar cell applications will not have transmission because of the metallic plate located at its back side. The selected geometry provides strong absorption at a certain frequency because of the structural properties which minimizes the reflection for the applied incident EM wave. This is very important for solar cell applications since more solar energy will be generated when the perfect absorption is obtained. In addition, the effects of the polarization angle on the behavior of the high-frequency structures are also important and it is examined both for infrared and visible frequency ranges. The frequency response of the absorption behavior can be seen in Figure 10. It can be clearly seen that the proposed MAs provide abundant absorption response for various polarization angles. There are very small frequency shifts depending on the angle changes and these shifts are in the negligible level. The absorption levels are not affected from the polarization angle variations and the same behaviors are observed as in the microwave structure (comparing to result of Figure 7). This means that no additional components/systems are needed to have a high-level absorption with polarization angle independency.

In order to verify the physical mechanism of the operation principle of the solar cell based on MTM at the resonances, the electric field and surface current distributions are investigated at the resonant frequencies and the results are shown in Figure 11 and Figure 12. In Figure 11, for $f = 4.28\,\text{GHz}$, the electric field concentrates around the splits of square loop for both front and back-sides. The electric field strongly couples with both side of the overall structure and induces free electric response. Hence, the surface charges are activated with electric field and create magnetic response and resonant absorption. Corresponding current distribution in Figure 12 for this resonance frequency includes both parallel and anti-parallel currents which cause electric and magnetic responses, respectively. These currents are excited by magnetic and/or electric coupling and induce magnetic and/or electric responses to couple

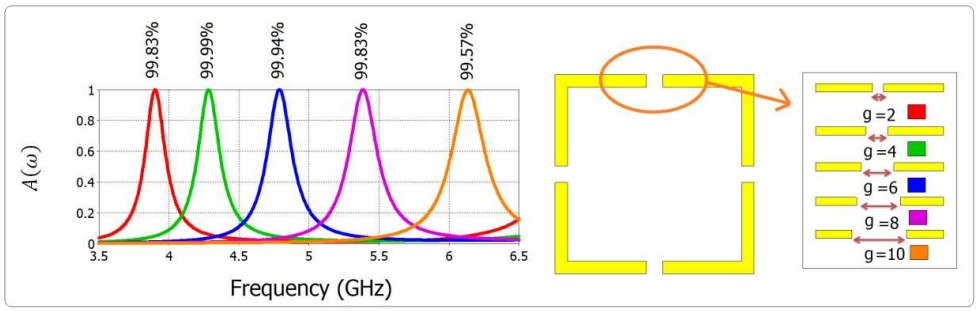

Figure 9. Absorption spectra for different gap values of the structure ($g = 2$, 4, 6, 8, and 10 mm).

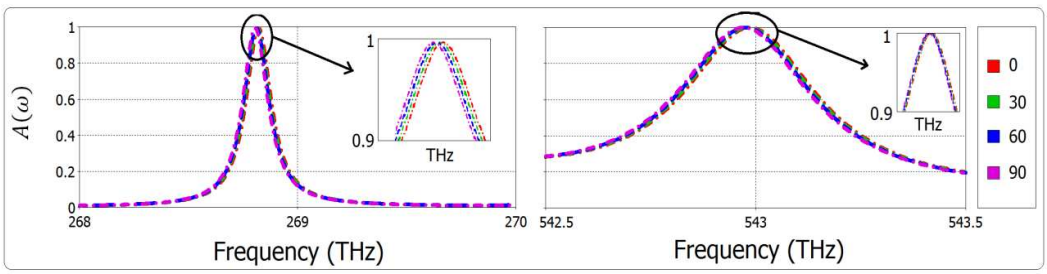

Figure 10. Simulated results of the absorbing performance under different polarization angles for both infrared and visible frequency ranges.

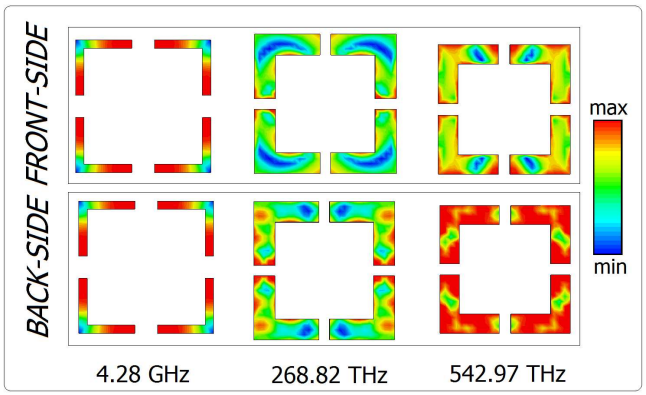

Figure 11. Electric field distributions at the resonant frequencies of the unit cell for microwave, infrared, and visible frequency regions.

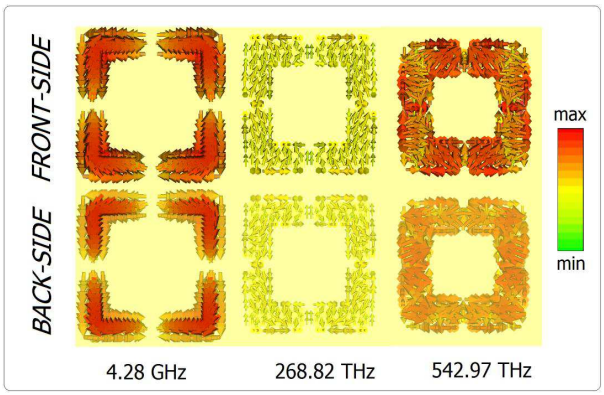

Figure 12. Surface current distributions at the resonant frequencies of the unit cell for microwave, infrared, and visible frequency regions.

with the externally applied field. Hence, at the resonance frequency, local response field is created and it builds up perfect absorption of incident radiation in the case of impedance matching condition ($Z(\omega) = Z_0(\omega)$). Therefore, whole incident energy is confined in the absorber that means reflection is minimized on the contrary of absorption. Electric field distribution for the second resonance frequency, which can be seen in the mid-section of Figure 11, is concentrated mostly around the horizontal gaps and the corresponding current distribution in the mid-section of Figure 12 is proportionally distributed. In other words, at this frequency point, electric and magnetic resonances are also occurred. Even though the absorbance level is perfect at this range, the character of the mode is different than the others. Similar physical mechanisms are valid for this resonance too. In the right side of Figure 11, third resonance, one can see that the electric field distribution is concentric at the edges of the front-side of the structure and there is a strong electric field at the back side of the structure. Currents accumulate at around the gaps for both horizontal and vertical sections. Strong accumulation of the currents causes an electric resonance and the current circulation yields a magnetic response. Hence, an absorption behavior can be observed.

5. CONCLUSION

The absorption properties of MA composed of square ring with four gaps are studied and discussed based on the experimental and simulation results and scrutinized with respect to its performance in microwave range. In addition, high frequency MAs are designed and simulated at both for infrared and visible frequency regions. The proposed absorber has simple geometry and reveals efficient results for microwave range and it is easily adopted for higher frequencies for applications of solar cells. The experimental results are in a good agreement with the numerical ones for microwave range. Both the simulated and measured absorption values are close to unity ($\gg 99\%$) for all resonances. It means that the performance of the simple geometry is perfect for various regions of the EM spectrum covers wide range of frequencies. According to the results, one can conclude that the proposed configurations can be used for solar cell applications. Moreover, the proposed configurations can also be modified to increase the efficiency of solar cells. Besides, it is demonstrated that the structure has polarization angle independency in all frequency regions which is very important for solar cells considering the overall day time. As a result, the structure can be used to design myriad absorbers for solar cells with polarization angle independency and it can be implemented/adopted to many frequency ranges for various applications such as long-distance radio telecommunications, satellite communications transmissions, some Wi-Fi devices, some cordless telephones, some weather radar systems, medical imaging, sensors, etc.

REFERENCES

1. Dincer, F., "The analysis on photovoltaic electricity generation status, potential and policies of the leading countries in solar energy," *Renew. Sust. Energ. Rev.*, Vol. 15, 713–720, 2011.
2. Dincer, F., "Overview of the photovoltaic technology status and perspective in Turkey," *Renew. Sust. Energ. Rev.*, Vol. 15, 3768–3779, 2011.
3. Liu, Y., Y. Chen, J. Li, T. Hung, and J. Li, "Study of energy absorption on solar cell using metamaterials," *Sol. Energy*, Vol. 86, 1586–1599, 2012.
4. Meral, M. E. and F. Dincer, "A review of the factors affecting operation and efficiency of photovoltaic based electricity generation systems," *Renew. Sust. Energ. Rev.*, Vol. 15, 2176–2184, 2013.
5. Aslam, M. I. and S. M. Ali, "A wideband metamaterial absorber for solar cell applications," *Proceedings of International Conference on Energy and Sustainability*, 113–116, Karachi, Pakistan, 2013.
6. Elwi, T. A. and H. M. Al-Rizzo, "Fresnel lenses based on nano shell-silver coated silica array for solar cells applications," *Progress In Electromagnetics Research B*, Vol. 32, 263–282, 2011.
7. Hao, J., J. Wang, X. Liu, W. J. Padilla, L. Zhou, and M. Qiu, "High performance optical absorber based on a plasmonic metamaterial," *Appl. Phys. Lett.*, Vol. 96, 251104-3, 2010.
8. Tao, H., C. M. Bingham, A. C. Strikwerda, D. Pilon, D. Shrekenhamer, N. I. Landy, K. Fan, X. Zhang, W. J. Padilla, and R. D. Averitt, "Highly flexible wide angle of incidence terahertz metamaterial absorber: Design, fabrication, and characterization," *Phys. Rev. B*, Vol. 78, No. 24, 241103-4, 2008.
9. Shen, X., T. J. Cui, J. Zhao, H. F. Ma, W. X. Jiang, and H. Li, "Polarization-independent wide-angle triple-band metamaterial absorber," *Opt. Express*, Vol. 19, No. 10, 9401–9407, 2011.
10. Liu, X., T. Tyler, T. Starr, A. F. Starr, N. M. Jokerst, and W. J. Padilla, "Taming the blackbody with infrared metamaterials as selective thermal emitters," *Phys. Rev. Lett.*, Vol. 107, No. 4, 045901-4, 2011.
11. Kao, T. S., F. M. Huang, Y. Chen, E. T. F. Rogers, and N. I. Zheludev, "Metamaterial as a controllable template for nanoscale field localization," *Appl. Phys. Lett.*, Vol. 96, No. 4, 041103-3, 2010.
12. Lin, C. H., R. L. Chern, and H. Y. Lin, "Polarization-independent broad-band nearly perfect absorbers in the visible regime," *Opt. Express*, Vol. 19, No. 2, 415–424, 2011.
13. Guo, W., L. He, B. Li, T. Teng, and X. W. Sun, "A wideband and dual-resonant terahertz metamaterial using a modified SRR structure," *Progress In Electromagnetics Research*, Vol. 134, 289–299, 2013.
14. Sabah, C. and S. Uckun, "Multilayer system of Lorentz/Drude type metamaterials with dielectric slabs and its application to electromagnetic filters," *Progress In Electromagnetics Research*, Vol. 91, 349–364, 2009.
15. Faruque, M. R. I., M. T. Islam, and N. Misran, "Design analysis of new metamaterial for EM absorption reduction," *Progress In Electromagnetics Research*, Vol. 124, 119–135, 2012.
16. Sabah, C., H. T. Tastan, F. Dincer, K. Delihacioglu, M. Karaaslan, and E. Unal, "Transmission tunneling through the multi-layer double-negative and double-positive slabs," *Progress In Electromagnetics Research*, Vol. 138, 293–306, 2013.
17. Huang, L. and H. Chen, "Multi-band and polarization insensitive metamaterial absorber," *Progress In Electromagnetics Research*, Vol. 113, 103–110, 2011.
18. Dincer, F., C. Sabah, M. Karaaslan, E. Unal, M. Bakir, and U. Erdiven, "Asymmetric transmission of linearly polarized waves and dynamically wave rotation using chiral metamaterial," *Progress In Electromagnetics Research*, Vol. 140, 227–239, 2013.

19. Zhu, B., Z. Wang, C. Huang, Y. Feng, J. Zhao, and T. Jiang, "Polarization insensitive metamaterial absorber with wide incident angle," *Progress In Electromagnetics Research*, Vol. 101, 231–239, 2010.
20. Li, M. H., H. L. Yang, and X. W. Hou, "Perfect metamaterial absorber with dual bands," *Progress In Electromagnetics Research*, Vol. 108, 37–49, 2010.
21. He, X. J., Y. Wang, J. M. Wang, and T. L. Gui, "Dual-band terahertz metamaterial absorber with polarization insensitivity and wide incident angle," *Progress In Electromagnetics Research*, Vol. 115, 381–397, 2011.
22. Nikooei Tehrani, K., A. Abdolali, D. Zarifi, and F. Hojjat-Kashani, "Application of chiral layers and metamaterials for the reduction of radar cross section," *Progress In Electromagnetics Research*, Vol. 137, 759–773, 2013.
23. Zarifi, D., H. Oraizi, and M. Soleimani, "Improved performance of circularly polarized antenna using semi-planar chiral metamaterial covers," *Progress In Electromagnetics Research*, Vol. 123, 337–354, 2012.
24. Vesalago, V. G., "The electrodynamics of substances with simultaneously negative values of ε and μ," *Sov. Phys. Usp.*, Vol. 10, 509–514, 1968.
25. Schurig, D., J. J. Mock, B. J. Justice, S. A. Cummer, J. B. Pendry, A. F. Starr, and D. R. Smith, "Metamaterial electromagnetic cloak at microwave frequencies," *Science*, Vol. 314, No. 5801, 977–980, 2006.
26. Fang, N., H. Lee, C. Sun, and X. Zhang, "Sub-diffraction-limited optical imaging with a silver superlens," *Science*, Vol. 308, No. 5721, 534–537, 2005.
27. Tao, H., N. I. Landy, C. M. Bingham, X. Zhang, R. D. Averitt, and W. J. Padilla, "A metamaterial absorber for the terahertz regime: Design, fabrication and characterization," *Opt. Express*, Vol. 16, No. 10, 7181–7188, 2008.
28. Johnson, P. B. and R. W. Christy, "Optical constants of the noble metals," *Phys. Rev. B*, Vol. 6, No. 12, 4370–4379, 1972.
29. Ordal, M. A., L. L. Long, R. J. Bell, S. E. Bell, R. R. Bell, R. W. Alexander, Jr., and C. A. Ward, "Optical properties of the metals Al, Co, Cu, Au, Fe, Pb, Ni, Pd, Pt, Ag, Ti, and W in the infrared and farinfrared," *Appl. Optics*, Vol. 22, No. 7, 1099–1119, 1983.
30. Sabah, C. and H. G. Roskos, "Effect of the Metallization on the resonances of THz fishnet metamaterials," *J. Eur. Opt. Soc. — Rapid Publ.*, Vol. 7, 12005, 2012.
31. Sabah, C. and H. G. Roskos, "Dual-band polarization-independent sub-terahertz fishnet metamaterial," *Curr. Appl. Phys.*, Vol. 12, 443–450, 2012.
32. Wanghuang, T., W. Chen, Y. Huang, and G. Wen, "Analysis of metamaterial absorber in normal and oblique incidence by using interference theory," *AIP Adv.*, Vol. 3, 102118-9, 2013.
33. Chen, H. T., J. F. Zhou, J. F. O. Hara, F. Chen, A. K. Azad, and A. J. Taylor, "Antireflection coating using metamaterials and identification of its mechanism," *Phys. Rev. Lett.*, Vol. 105, No. 7, 073901-4, 2010.
34. Chen, H. T., "Interference theory of metamaterial perfect absorbers," *Opt. Express*, Vol. 20, No. 7, 7165–7172, 2012.
35. Jackson, J. D., *Classical Electrodynamics,* 3rd Edition, Wiley-VCH, Jul. 1998.
36. Sabah, C., "Tunable metamaterial design composed of triangular split ring resonator and wire strip for S- and C-microwave bands," *Progress In Electromagnetics Research B*, Vol. 22, 341–357, 2010.